



# Understanding structural changes in NMC Li-ion cells by *in situ* neutron diffraction



O. Dolotko<sup>a,b,\*</sup>, A. Senyshyn<sup>b</sup>, M.J. Mühlbauer<sup>a,b,c</sup>, K. Nikolowski<sup>a,c</sup>, H. Ehrenberg<sup>a,c,d</sup>

<sup>a</sup> Materials Science, Technische Universität Darmstadt, Petersenstrasse 23, D-64287 Darmstadt, Germany

<sup>b</sup> Forschungs-Neutronenquelle Heinz Maier-Leibnitz FRM II, Technische Universität München, Lichtenbergstrasse 1, D-85748 Garching b. München, Germany

<sup>c</sup> Karlsruhe Institute of Technology (KIT), Institute for Applied Materials-Energy Storage Systems (IAM-ESS), Hermann-von-Helmholtz-Platz 1, D-76344 Eggenstein-Leopoldshafen, Germany

<sup>d</sup> Helmholtz-Institute Ulm for Electrochemical Energy Storage (HIU), P.O. Box 3640, D-76021 Karlsruhe, Germany

## HIGHLIGHTS

- NMC cell was studied *in-situ* using neutron diffraction and electrochemistry.
- Transformation of the anode into  $\text{LiC}_6$  and  $\text{LiC}_{12}$  was found in higher charge states.
- A change of the Li occupation and lattice parameters in the cathode were observed.
- The cation mixing in the cathode vanishes if the cell capacity is above  $\sim 0.8Q_{\text{max}}$ .
- The cation mixing can be one of the reasons of nonlinear lattice parameter changes.

## ARTICLE INFO

### Article history:

Received 22 July 2013

Received in revised form

9 December 2013

Accepted 3 January 2014

Available online 9 January 2014

### Keywords:

Li-ion

NMC cell

*In situ* study

Electrodes

Neutron powder diffraction

## ABSTRACT

Commercial NMC cells of 18650-type based on a  $\text{Li}_x(\text{Ni}_{0.5}\text{Mn}_{0.3}\text{Co}_{0.2})\text{O}_2$  cathode and a graphitic anode were studied *in situ* using a combination of high-resolution monochromatic neutron powder diffraction and electrochemical analysis. The structural changes of the electrode materials during cell charge/discharge have been determined using Rietveld refinement and single profile decomposition techniques. A transformation of the graphitic anode to  $\text{LiC}_{12}$  and  $\text{LiC}_6$  through the formation of higher ordered lithium intercalated carbons was observed. A different behavior of electrochemically-driven lattice distortion was observed for NMC material in comparison to  $\text{Li}_x\text{CoO}_2$  and its influence on the overall cell performance has been discussed in brief. Detailed analysis of the structural changes in the  $\text{Li}_x(\text{Ni}_{0.5}\text{Mn}_{0.3}\text{Co}_{0.2})\text{O}_2$  cathode material revealed reversible Li/Ni cation mixing (5.6(8)%), which is state-of-charge independent below 1600 mAh and vanishing above 1800 mAh ( $\sim 0.8Q_{\text{max}}$ ).

© 2014 Elsevier B.V. All rights reserved.

## 1. Introduction

Applications of Li-ion batteries vary broadly from supplying small devices to powering hybrid electric vehicles. Despite their overall success, nowadays it is widely recognized that further critical breakthroughs in science and technology of Li-ion battery materials are necessary to develop lower-cost, longer-life, higher energy/power density batteries. Among different factors the electrochemical performance of the positive electrode (cathode) is

often believed to be the bottleneck for the stable operation of the overall Li-ion cell. The major part of the cathode materials used in state-of-the-art Li-ion cells is primarily based on three prototypes, namely  $\text{LiMeO}_2$  layered oxide, olivine-type  $\text{LiMePO}_4$  and spinel-type  $\text{LiMe}_2\text{O}_4$ , where Me is a transition metal. Each material depending on its chemical composition, preparation route and morphology possesses its own advantages and drawbacks (analyzed in detail elsewhere [1–19]).

In the current contribution the main focus is on the  $\text{LiMeO}_2$  layered oxides, whose representative  $\text{LiCoO}_2$  (LCO) is widely used as cathode material for the majority of so-called high-energy Li-ion cells currently present on the market. In spite of its spreading the  $\text{LiCoO}_2$  suffers from a poor safety at elevated temperature in the fully charged state, its high cost, toxicity of cobalt, and a rather low capacity, because only 50% of the Li can be exploited. The challenges

\* Corresponding author. Forschungs-Neutronenquelle Heinz Maier-Leibnitz FRM II, Technische Universität München, Lichtenbergstrasse 1, D-85748 Garching b. München, Germany. Tel.: +49 89 289 14373; fax: +49 89 289 14911.

E-mail address: [sdolotko@yahoo.com](mailto:sdolotko@yahoo.com) (O. Dolotko).

associated with  $\text{LiNiO}_2$  include difficulties in preparation of stoichiometric powders, structural instability during electrochemical cycling along with thermal safety problems caused by oxygen release in the charged state. A drawback of  $\text{LiMnO}_2$  is its crystallographic transformation from layered to spinel structure in the charged state.

A variety of efforts have been undertaken over the past decade to improve the performance of the  $\text{LiMeO}_2$ -type cathode materials. The introduction of mixed transition metal  $\text{Li}(\text{Ni}, \text{Mn}, \text{Co})\text{O}_2$  (NMC) oxides allows for a combination of advantages offered by different  $\text{LiMeO}_2$  layered oxides paving the way towards less toxicity, improved thermal stability in charged state, better cycling stability even at elevated temperatures, higher reversible capacity, lower costs etc. A large diversity of  $\text{Li}(\text{Ni}, \text{Mn}, \text{Co})\text{O}_2$  compositions was synthesized, characterized and tested as possible electrode materials for NMC Li-ion cells in the past [20–30].

The presence of different transition metals results in their complicated interaction upon Li de/intercalation, e.g. at different charge states of the cell the transition metals in the NMC cathode are present in different oxidation states, namely  $\text{Ni}^{2+}$ ,  $\text{Ni}^{4+}$ ,  $\text{Co}^{3+}$ ,  $\text{Co}^{4+}$  and  $\text{Mn}^{4+}$ . The  $\text{Ni}^{2+}/\text{Ni}^{4+}$  couple is responsible for most of the cycling capacity up to de/intercalation of 2/3Li per formula unit, and the  $\text{Co}^{3+}/\text{Co}^{4+}$  couple is mainly involved in the range  $2/3 \leq x \leq 1$  in the  $\text{Li}_{1-x}\text{Ni}_{1/3}\text{Mn}_{1/3}\text{Co}_{1/3}\text{O}_2$  cathode, while the  $\text{Mn}^{4+}$  is believed to be electrochemically inactive and stabilizing the crystal structure [31,32].

This complex character of the interactions between transition metals results in a cation mixing effect – an antisite disorder between lithium and a transition metal. In most cases the cation mixing is reflected in the interchange between a  $\text{Li}^+$  ion and a nearest neighbor  $\text{Ni}^{2+}$  ion on the crystallographic 3a and 3b sites of the NMC lattice (ensuring local charge neutrality/minimization of Coulomb energy). It is known to deteriorate the electrochemical performance of layered oxides [33–35]. A partial occupation of  $\text{Li}^+$  lattice sites by  $\text{Ni}^{2+}$  (having similar ionic radii) blocks the lithium diffusion pathway on a short-range scale and, therefore, a number of recently published investigations focus on the minimization of this effect by overlithiation [36–40]. On the other hand the cation mixing had also been found seriously influenced by the chemical composition (ratio of transition metals), e.g. evidently low cation mixing in NMC materials with decreased nickel contents was reported in Refs. [30,35]. Authors [40–42] reported a decrease (or total removal) of Ni atoms on Li sites (3a) by increasing the Co content in NMC material.

The literature data on cation mixing in NMC materials (especially for high nickel contents as well as its behavior at different lithium contents) have been found quite limited and somewhat controversial. For data based on X-ray diffraction authors [43] reported the suppression of cation mixing in  $\text{Li}(\text{Ni}_{0.5}\text{Mn}_{0.3}\text{Co}_{0.2})\text{O}_2$  by increasing the oxygen content in preparing atmosphere. In Ref. [41] no traces of cation mixing were observed in  $\text{Li}(\text{Ni}_{0.6}\text{Mn}_{0.4-x}\text{Co}_x)\text{O}_2$  ( $x = 0.05, 0.1, 0.15, 0.2$ ). Ma et al. [29] concluded 4.4% Ni on Li site and vice versa for  $\text{Li}(\text{Ni}_{0.4}\text{Mn}_{0.4}\text{Co}_{0.2})\text{O}_2$ , whereas for the sample with  $\text{Li}(\text{Ni}_{0.425}\text{Mn}_{0.425}\text{Co}_{0.15})\text{O}_2$  nominal composition the Ni on 3a site along with no lithium on transition metal site was detected [36]. The stability of the cation mixing at different lithium contents creates a substantial matter for discussions, e.g. authors [44,45] have found that the cation mixing in  $\text{Li}_x\text{Ni}_{0.5}\text{Mn}_{0.5}\text{O}_2$  is essentially constant, whilst in Refs. [46,47] it was shown that Li ions are removed from transition metal sheets early on charging. Idemoto et al. [48] studying  $\text{Li}_x\text{Ni}_{0.8}\text{Co}_{0.2}\text{O}_2$  ( $x = 0.4–1.1$ ) have concluded that the cation mixing occurs at the time of synthesis and undergoes no significant modifications upon charge/discharge.

It should be emphasized that the majority of structural studies on NMC cathodes are based on *ex situ* techniques, which, in theory,

may lead to some uncontrolled deviations from the genuine state due to possible materials oxidation, cell charge changes, electrolyte evaporation/decomposition etc. Much authoritative information can be achieved by the characterization of electrode materials under real operating conditions, where use of high-energy X-ray or synchrotron powder diffraction can provide information about unit cell dimensions change, presence of cation mixing or morphology change upon battery cycling [49–52]. However, there is a limited capability for Li detection due to low scattering power of light elements and a restricted possibility to distinguish between neighboring elements in the periodic table confines the accuracy of *in situ* XRD analysis.

In this sense by neutron powder diffraction (NPD) can achieve a much better experimental “figure of merit”, where isotope-sensitive neutron scattering permits accurate distinction of elements with close atomic numbers, like Ni, Co and Mn and localization of light elements (Li and O). The neutron scattering lengths (not depending on momentum transfer  $\sin(\theta)/\lambda$ ) often give more accurate lattice parameters and Debye–Waller factors in comparison to X-ray diffraction. Their low energy along with a high penetration depth makes thermal neutrons a universal tool for non-destructive structural studies.

The only drawback for *in situ* NPD battery investigation is the presence of hydrogen-containing components, namely the separator and liquid electrolyte, which result in a high incoherent background and in an enhanced neutron attenuation. Numerous attempts of designing the custom built neutron and diffraction-friendly primary and secondary cells, where hydrogen-containing components are either replaced by deuterated alternatives or equivalents containing less or no hydrogen have been reported [13–16,53–56]. Authors [12,57] used cells with reduced amount of hydrogen for investigations of  $\text{LiCoO}_2$ ,  $\text{LiMn}_2\text{O}_4$ ,  $\text{LiFePO}_4$  and  $\text{MoS}_2$  positive electrode materials.

Despite of all experimental difficulties there is increased amount of scientific groups which use the *in situ* neutron diffraction for electrode materials characterization in commercial cells of different types and geometries, which have the advantage of being extremely industrially relevant. Recent publications of *in situ* NPD studies on the commercial batteries have been undertaken for the cells with  $\text{LiCoO}_2$  [4,58–63],  $\text{LiFePO}_4$  [11,64] and spinel  $\text{LiMn}_2\text{O}_4$  [17,65] cathodes, where the evolution of the crystal structure of anode and cathode materials versus state-of-charge (SOC) or fatigue (state-of-health, SOH) was investigated. The *in situ* neutron diffraction analysis was also successfully applied to identify details of the lithium intercalation process into the graphitic anode of commercial 18650-type LCO [62,66] and pouch bag-type NMC [67] cells.

In the current contribution *in situ* high-resolution neutron powder diffraction along with electrochemical analysis is applied to study the cation mixing process in Ni-rich NMC material. In order to achieve real operating conditions the experiment is performed on a cylindrical 18650-type NMC based Li-ion cell during electrochemical charge/discharge in the nominal voltage window.

## 2. Experimental

A commercial cylindrical rechargeable NMC Li-ion cell with a  $\text{Li}(\text{Ni}_{0.5}\text{Mn}_{0.3}\text{Co}_{0.2})\text{O}_2$  cathode and a graphite anode with nominal capacity of 2200 mAh was studied. A VMP3 multichannel potentiostat from Bio-Logic was applied to charge and discharge the cell (3.0–4.2 V, CCCV, 0.18C, 400 mA current). Neutron powder diffraction patterns were collected during the cycling process. The first set of experimental data was collected during a constant charge–discharge of the cell in the voltage window of 3.0 V–4.2 V.

The exposure time per single NPD pattern was approx. 30 min, further described as “continuous”. A second data set was collected at different equilibrated SOC for 4 h each, further described as “equilibrated”. A third set of data was collected at a constant current of 400 mA during the changes between the different SOC. The neutron powder diffraction experiments were performed at the high-resolution powder diffractometer SPODI [68] at ambient temperature using monochromatic neutrons with  $\lambda = 1.5483(1)$  Å. Its vertical position-sensitive multidetector consists of 80  $^3\text{He}$  tubes with an effective height of 300 mm and covers an angular range of  $2\theta$  from  $0^\circ$  to  $160^\circ$ . All measurements were performed in Debye–Scherrer geometry with an incident neutron beam having a rectangular cross section at the sample position of  $40 \times 30 \text{ mm}^2$ . In order to reduce the background and to improve the transmission characteristics of the sample the plastic cover has been removed from the battery prior to the mounting of the cell on the sample table of the diffractometer. To avoid the unwanted gasket, pressure vents and contacts contributions to the resulting powder diffraction pattern, the upper and bottom parts of the battery (10 mm) were covered by 0.5 mm thick cadmium foil.

Rietveld refinement has successfully been applied to characterize the structure of the positive and negative electrodes and of the current collectors using the FullProf software package [69]. A single profile decomposition technique has been used for the treatment of diffraction peaks obtained from short scans during the “continuous” and “equilibrated” constant charge–discharge processes. The single profile decomposition has been applied to Bragg reflections of the investigated phases, which do not overlap with the others. For this purpose two Bragg reflections 003 and 217 of  $\text{Li}_x(\text{Ni}_{0.5}\text{Mn}_{0.3}\text{Co}_{0.2})\text{O}_2$  have been selected. A Gaussian peak shape has been assumed resulting in parameters for position, intensity and full width half maximum of the examined reflections. The lattice parameters were calculated from the 003 and 217 reflection positions.

“Equilibrated” data were fitted over the  $2\theta$  range from  $10^\circ$  to  $149^\circ$ . Due to heavy preferred crystallite orientations in a signal from the steel housing a structure independent (Le-Bail) profile fit was used. The background (shape and magnitude) of the recorded NPD patterns is similar for all SOC of the Li-ion cell and fitted using a linear interpolation between selected data points in non-overlapping regions. The Thompson–Cox–Hastings pseudo-Voigt function was used for the peak profile shape description. The instrumental resolution function was determined for a  $\text{Na}_2\text{Ca}_3\text{Al}_2\text{F}_{14}$  reference material and explicitly used for calculation of the reflections half widths. Additional peak broadening from the sample was taken into account as a phase-specific microstrain or in the case of graphite and the Li-intercalated carbons as a crystallite size effect.

The composition of the cathode material  $\text{Li}_x(\text{Ni}_{0.5}\text{Mn}_{0.3}\text{Co}_{0.2})\text{O}_2$  was confirmed quantitatively by the inductively coupled plasma optical emission spectroscopy (ICP-OES) method (IRIS Intrepid II XUV, Thermo Fisher). For this experiment the fully discharged NMC cell was dismantled in a glove box and a portion of cathode material was extracted from the current collector for further analysis.

### 3. Results and discussions

The noticeable relationship between neutron powder diffraction patterns and electrochemical state of charge was detected by *in situ* experiments on commercial lithium-ion cells. A series of patterns is shown in the form of 2D plot (time vs.  $2\theta$  angle with logarithm intensities as grayscale) in Fig. 1.

Changes in the scattering angle of the reflections from positive and negative electrodes are monitored as a function of time and related to the electrochemical cell characteristics (capacity). The

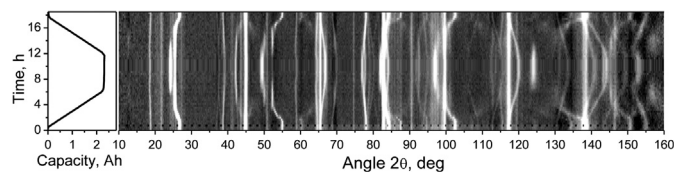


Fig. 1. Time evolution of neutron powder diffraction patterns collected for a commercial Li-ion NMC cell of 18650-type as function of the cell state (capacity).

observed high background is primarily induced by the incoherent scattering of hydrogen in the electrolyte and the separator. The background shows a nonlinear behavior, caused by the high neutron absorption cross sections of lithium and cobalt and is independent from the SOC. Therefore, background subtraction procedure was applied to data shown in Fig. 1.

In general the obtained neutron powder diffraction signal can be separated into the  $\text{Li}_x(\text{Ni}_{0.5}\text{Mn}_{0.3}\text{Co}_{0.2})\text{O}_2$  positive electrode, the graphite negative electrode (in discharged state) or lithium intercalated carbons ( $\text{LiC}_{12}$  and  $\text{LiC}_6$ , in charged state), copper and aluminum as current collectors and  $\alpha$ -Fe from the housing (Fig. 2). The separator contribution to the diffraction patterns results in two reflections in the NPD patterns occurring in the  $21^\circ$ – $22.2^\circ$  and  $40.5^\circ$ – $41.5^\circ$   $2\theta$ -ranges, whose properties were found independent on the SOC.

#### 3.1. Negative electrode (graphite) behavior

The lithium intercalation into the graphite-based electrode results in the formation of lithium intercalated graphite structures [70,71] coexisting in carbon–lithium binary system in the form of stages [72,73]. Recent studies of  $\text{LiCoO}_2|\text{C}|$  based Li-ion cell of 18650-type applying *in-situ* high-resolution NPD and electrochemical characterization revealed some new details to the Li intercalation mechanism into the graphite [62]. Behavior of the graphite negative electrode upon de/lithiation in the current cell has been found consistent with results reported in Ref. [62]. The lithium insertion into graphite can be illustrated on example of 001 ( $\text{LiC}_6$ ) and 002 ( $\text{LiC}_{12}$  and C) reflection evolution whose intensities and positions are strongly influenced by SOC (Fig. 3). At 100% SOC

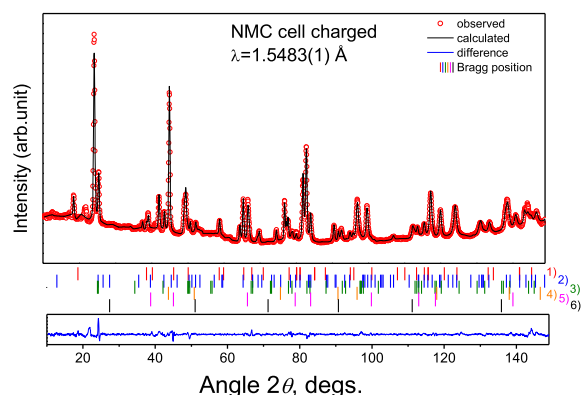


Fig. 2. Example for the Rietveld refinement of the structure models, based on neutron powder diffraction data of the NMC cell of 18650-type in charged state. Vertical bars placed in rows (1–6) mark calculated positions of Bragg peaks of the refined phases: (1, red) – cathode  $\text{Li}_x(\text{Ni}_{0.5}\text{Mn}_{0.3}\text{Co}_{0.2})\text{O}_2$ ; (2, blue; 3, green) – lithium intercalated carbons  $\text{LiC}_{12}$  and  $\text{LiC}_6$  respectively; (4, orange) – copper current collector; (5, pink) – aluminum current collector; (6, black) – steel housing. (For interpretation of the references to color in this figure legend, the reader is referred to the web version of this article.)

both stage I ( $\text{LiC}_6$ ) and stage II ( $\text{LiC}_{12}$ ) are coexisting; cell discharge results in the reduction of the stage I fraction while there is an increase of the stage II fraction and at  $Q \sim 1400$  mAh the stage I vanishes. At 1200 mAh cell capacity the position of 002 reflection for  $\text{LiC}_{12}$  was already found shifted from its nominal position in contradiction with its stage nature. Further reduction of cell capacity results in a continuous (quasi-Vegard) shift of the 002 reflection position upon  $\text{LiC}_{12}$ -to-C transformation, which is supplemented by nonlinear dependencies of the 002 reflection intensity and its width. The observation of this process is strongly limited by the experimental resolution, but in Ref. [62] this deviation was attributed to the formation of numerous  $\text{Li}_x\text{C}_6$  compositions with  $x_{\text{Li}} < 0.5$ , which are stable in certain capacity ranges and whose lattice parameter  $c$  is comparable to graphite.

### 3.2. Positive electrode behavior

Contrary to the negative electrode, which undergoes numerous phase transformations upon a complete lithium de/intercalation, the positive electrode material shows a single phase mechanism during cell charge/discharge. Structural analysis based on *in situ* data revealed a  $\alpha$ - $\text{NaFeO}_2$  type structure (space group R-3m) for  $\text{Li}_x(\text{Ni}_{0.5}\text{Mn}_{0.3}\text{Co}_{0.2})\text{O}_2$ . The basic structure of  $\text{LiMeO}_2$  is known to consist of sheets of  $\text{Me}^{3+}$ -based edge sharing  $\text{MeO}_6$  octahedra separated by sheets of  $\text{Li}^+$ , where Me is a transition metal or their combination. The  $\text{Li}^+$  ions occupy octahedral cavities between the oxygen of adjacent metal oxide layers. In  $\alpha$ - $\text{NaFeO}_2$  type structures the  $\text{MeO}_2$  layers are stacked in an ABCABC fashion, where the unit cell of  $\text{LiMeO}_2$  contains three layers in the hexagonal setting of the rhombohedral structure [74].

#### 3.2.1. Lattice parameter analysis

Upon cell charge/discharge the lithium extraction/insertion leads to a distortion of the structure of the NMC material reflected in shifts of its peak positions. In Fig. 3 the two Bragg reflections 003 and 217 (representing structural changes of the  $\text{Li}_x(\text{Ni}_{0.5}\text{Mn}_{0.3}\text{Co}_{0.2})\text{O}_2$  upon battery charging and not overlapping with other peaks) are shown. A shift of the 003 reflection position towards smaller  $2\theta$  values at the beginning of the charge process corresponds to an expansion of the unit cell in  $c$  direction. The 217 reflection, containing contributions from both  $a$  and  $c$  lattice parameters, displays the opposite behavior, indicating a simultaneous shrinking of the  $a$  cell dimension. A relatively narrow capacity range of existence for

stage I and stage II intercalated carbons results in a non overlapping with 217 reflection from NMC, whose position is highly dependent on the SOC.

The evolution of the  $\text{Li}_x(\text{Ni}_{0.5}\text{Mn}_{0.3}\text{Co}_{0.2})\text{O}_2$  lattice parameters as a function of the cell capacity is plotted in Fig. 4. A comparison of the observed lattice parameters determined via single profile decomposition of 003 and 217 reflections and a full profile Rietveld analysis (see below) have been found in fair agreement, but revealing some minor deviations due to the fact that data have been acquired in a “continuous” and an “equilibrated” mode. Differences are a measure for the magnitude of relaxation effects on the underlying structures. However, independently from the method of data treatment the general changes of the lattice parameter remain similar.

The slope of the curve describing the lattice parameter  $a$  decreases upon battery charging and becomes nearly zero above 1800 mAh (Fig. 4). A similar behavior was observed for  $\text{LiCoO}_2$  (the data was taken from Ref. [62], where only the anode behavior was reported in detail). The lattice parameter  $a$  of the  $\text{LiCoO}_2$  undergoes a decrease by  $-0.7\%$  upon charging, which is obviously less than the corresponding decrease in the NMC material ( $-1.6\%$ ).

In the capacity range 0–2200 mAh the LCO lattice parameter  $c$  linearly increases upon charging (lithium removal) and becomes nearly capacity independent at  $Q > 2200$  mAh (ca. 85% of SOC). The lattice parameter of NMC undergoes similar trend upon charge: it raises in a linear fashion first, goes through its maximum at 1800 mAh ( $0.80Q_{\text{max}}$ ) and, in contrast to LCO, the NMC lattice parameter  $c$  shows a decrease at capacities above 1800 mAh. The lattice parameter  $c$  of the  $\text{LiCoO}_2$  undergoes an increase by 2.5% upon charging, whereas the NMC material shows an increase of  $c$  lattice parameter by 1.5%. This increase of lattice parameter  $c$  in both LCO and NMC materials upon lithium removal can be explained by the electrostatic repulsion of the oxygen layers that is only partly screened when lithium sites are not fully occupied [75], which corresponds to a cathode unit cell deformation [25,29,31,39]. On the other hand in  $\text{Li}_x\text{MeO}_2$  materials a decrease of lattice parameter  $c$  is expected at  $x_{\text{Li}} < 0.4$  [3,5,75] due to a change in the charge distribution. The average charge at the oxygen ions is expected to decrease when the lithium content is lowered, which may cause a decrease of the repulsion between oxygen layers and, consequently, shortening of interlayer distances. Taking into account the obtained lithium occupation  $x_{\text{Li}}$  of 0.26(3) and 0.50(2) [61] for NMC and LCO electrodes in fully charged states, no maximum of  $c$  lattice parameter is expected to occur for LCO material. However further delithiation may lead to the decrease of the  $c$  lattice parameter [3,5,75].

In both NMC and LCO the opposite behavior of  $a$  and  $c$  lattice parameters was observed which leads to a minimized change of the unit cell volume ( $-2.2\%$  and  $+1.9\%$  upon cell charge, respectively). Taking into account the polycrystalline form of the electrode materials used along with the increasing cell volume of  $\text{Li}_x\text{C}_6$  anode upon lithium intercalation the observed behavior of cell volume might be advantageous for the minimization of the overall volume change of the working cell and for the reduction of mechanical stresses.

#### 3.2.2. Cation mixing and bond length analysis

In the  $\text{Li}_x(\text{Ni}_{0.5}\text{Mn}_{0.3}\text{Co}_{0.2})\text{O}_2$  structure some of the Ni atoms were found on the lithium layer on the 3a site (0, 0, 0) along with partial Li-occupation of the Ni layer on the 3b site (0, 0,  $\frac{1}{2}$ ). As it was mentioned above this effect was reported to occur in a number of nickel-containing electrode materials with distorted rocksalt structure [29,36,43] and the diffraction methods are often used there to quantify the cation mixing. Unfortunately, the powder

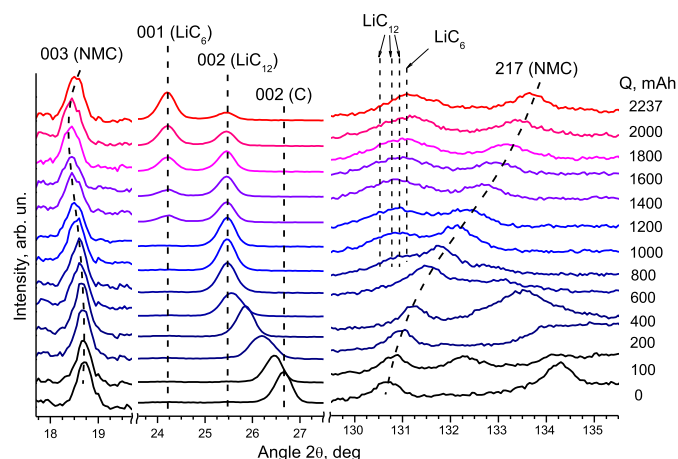
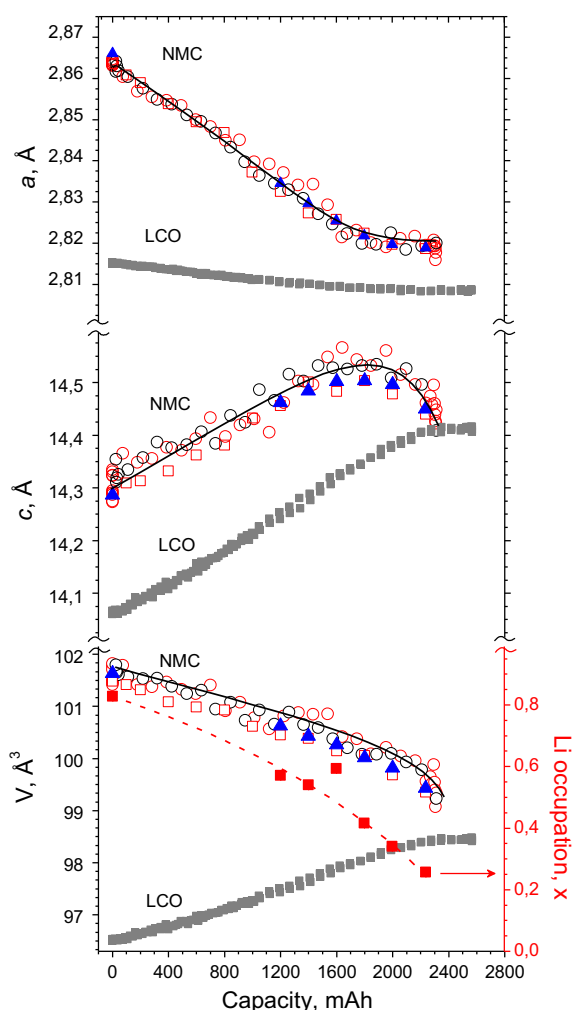


Fig. 3. Enlarged sections of neutron diffraction patterns obtained from a commercial 18650-type NMC Li-ion cell upon different “equilibrated” charge states. Dashed lines are guides for the eyes.



**Fig. 4.** Evolution of the  $\text{Li}_x(\text{Ni}_{0.5}\text{Mn}_{0.3}\text{Co}_{0.2})\text{O}_2$  lattice parameters and Li occupation as a function of the cell capacity. Red and black empty circles correspond to the two reflections 003 and 217 and are obtained by single profile decomposition of the "continuous" data taken during charge (red) and discharge (black) of the cell. Red empty squares result from fitting the two peaks 003 and 217 for the "equilibrated" data; blue triangles from a refinement of the full powder diffraction pattern for the "equilibrated" data. Grey squares show data of a LCO cell for comparison. Red filled squares finally indicate the Li occupation in the structure of the cathode. Lines are guides for the eyes. (For interpretation of the references to color in this figure legend, the reader is referred to the web version of this article.)

diffraction analysis based on a least-square minimization of the differences between observed and calculated profiles from NMC material with cation mixing, does not permit independent determination of Li and Ni distribution over 3a and 3b atomic sites. This is caused by the ill-defined relationship between scattering factors

and site occupancies, where only overall lithium occupation (and nickel if needed) can be determined from diffraction data with enough confidence. The accurate solution requires either use of independent input information or implementation of supplementary/supporting constraints.

Lab analytical methods (OCP, NMR, XRD) usually serve as an independent *ex-situ* input for NMC studies. However, their application is hardly limited when the whole 18650-type cell is subjected to study. Therefore, the following constraints were applied as an alternative: the occupation factors  $g(\text{Mn})$  and  $g(\text{Co})$  on the 3b sites were fixed to 0.3 and 0.2 (relative fractions of the transitional metal site occupation, 1.0 corresponding to 100% occupation probability), respectively. The overall content of Ni was fixed as 0.5 per formula unit, but its distribution between 3a (Li1, Ni1) and 3b (Li2, Ni2) sites was constrained assuming  $g(\text{Li2}) = g(\text{Ni1})$  and  $g(\text{Ni1}) + g(\text{Ni2}) = 0.5$ . The only refined fractional coordinate was  $z/c$  of the oxygen atoms on the 6c site (0, 0, z).

The chosen kind of constraint (already applied for studies of cation mixing in NMC materials [29,32,44,45]) was found chemically reliable, results in no correlations and stable least-square minimization process. The general formula of the NMC material can then be written as:  $(\text{Li}_{x-x'}\text{Ni}_{x'}) (\text{Ni}_{0.5-x'}\text{Li}_{x'}\text{Mn}_{0.3}\text{Co}_{0.2})\text{O}_2$ , where  $x - x'$  and  $x'$  are the amounts of Li on the 3a and 3b sites, respectively.

The refined unit cell parameters, Li/Ni site occupancies and overall displacement parameters are listed in Table 1. An analysis of the crystal structure parameters at different SOC of  $(\text{Li}_{x-x'}\text{Ni}_{x'}) (\text{Ni}_{0.5-x'}\text{Li}_{x'}\text{Mn}_{0.3}\text{Co}_{0.2})\text{O}_2$  revealed an increase of the scattering power on the 3a site, interpreted as a removal of Li (possessing a negative scattering length). After reaching a SOC of 1800 mAh the lithium was found to be fully extracted from 3b positions along with no Ni atoms occupying the 3a site. Further electrochemical charging proceeds with no cation mixing where lithium and nickel atoms remain in their own atomic positions separated in 3a and 3b sites, respectively. A nonlinear dependence of lithium content  $x_{\text{Li}}$  in NMC material vs. cell capacity was observed and a sort of direct correlation to the observed capacity behavior for cell volume can be drawn.

At an initial state the delithiation of NMC material proceeds by removing  $\text{Li}^+$  ions from lithium sheets and leads to an increase of Li–O interatomic distance with simultaneous reduction of M–O interatomic distances (listed in Table 1). An increase of Li–O interatomic distances upon Li removal is typical for  $\text{Li}_x\text{MeO}_2$  materials and can be understood in line with the reduction of  $c$  lattice parameter upon Li intercalation mentioned above. An increase of the 3a–6c bond length along with the 3b–6c bond length decrease in the  $Q = 0$ –1800 mAh range upon delithiation is evident, whereas at  $Q > 1800$  mAh only a slight decrease of 3a–6c and an increase of the 3b–6c bond length during further delithiation was noticed.

**Table 1**

Evolution of structural parameters of the  $\text{Li}_x(\text{Ni}_{0.5}\text{Mn}_{0.3}\text{Co}_{0.2})\text{O}_2$  cathode in NMC commercial Li ion battery of 18650 type. Displacement parameters were modeled using  $B_{\text{ov}}$ , lithium occupation was allowed to vary; numbers in parentheses give statistical errors in the last significant digit. Figures of merit (not corrected for background)  $R_p$ ,  $R_{wp}$  and  $\chi^2$  correspond to profile, weighted profile residuals and goodness of fit, respectively.

Cell capacity, mAh	Lattice parameters		$c/a$	Li site occupancy $x_{\text{Li}}$ , frac. un.		$B_{\text{ov}}$ , Å	Bond length, Å		Oxygen coordinate (6c) $z/c$ , frac. un.	$R_p$ , $R_{wp}$ , $\chi^2$
	$a$ , Å	$c$ , Å		Li1 (3a)	Li2 (3b)		3a–6c	3b–6c		
0	2.86601(5)	14.28635(45)	4.98475(5)	0.77(3)	0.054(6)	1.17(5)	2.131(2)	1.954(1)	0.2394(2)	1.10 1.42 5.70
1200	2.83447(5)	14.46172(59)	5.10209(11)	0.52(5)	0.047(8)	1.14(5)	2.169(3)	1.911(2)	0.2349(3)	1.10 1.43 5.10
1400	2.82959(5)	14.48355(64)	5.11860(13)	0.48(4)	0.060(8)	1.42(5)	2.165(2)	1.912(2)	0.2352(2)	1.02 1.36 4.58
1600	2.82543(5)	14.50188(69)	5.13263(13)	0.53(4)	0.063(8)	1.07(6)	2.171(3)	1.906(2)	0.2346(3)	1.05 1.35 4.00
1800	2.82178(5)	14.50371(66)	5.13992(12)	0.42(4)	–	0.84(5)	2.153(3)	1.917(2)	0.2363(3)	1.07 1.38 5.35
2000	2.81970(5)	14.49633(62)	5.14109(12)	0.34(4)	–	0.84(5)	2.153(2)	1.914(2)	0.2361(2)	1.08 1.38 5.34
2237	2.81880(5)	14.44935(64)	5.12606(14)	0.26(3)	–	1.01(3)	2.150(2)	1.912(1)	0.2361(2)	1.14 1.48 6.01

#### 4. Conclusions

The *in situ* high-resolution neutron powder diffraction analysis was applied for investigation of structural changes in electrode materials related to the lithium intercalation/deintercalation in commercial Li-ion NMC (18650-type) cells. The lithium distribution in the anode and cathode structure in dependence of the SOC of the cell was investigated.

Transformation of graphitic anode into  $\text{LiC}_{12}$  and  $\text{LiC}_6$  stages through the formation of higher ordered lithium intercalated carbons upon cell charge was found consistent with the previous investigations on LCO cell [62]. At the same time the structural behavior of the  $\text{Li}_x(\text{Ni}_{0.5}\text{Mn}_{0.3}\text{Co}_{0.2})\text{O}_2$  cathode was found noticeably different to that of LCO. Upon cycling the lithium extraction/insertion distorts the  $\text{Li}_x(\text{Ni}_{0.5}\text{Mn}_{0.3}\text{Co}_{0.2})\text{O}_2$  cathode structure in a different way, which leads to the reduction (−2.2%) and increase (+1.9%) of cell volume in NMC and LCO material upon charging, respectively. According to the X-ray tomography (unpublished) the typical LCO-based 18650-type Li-ion cell undergoes ca. 100  $\mu\text{m}$  change of its outer diameter (cyclic strain) during CCCV charge/discharge (3.0–4.2 V, 0.4 A). The character of the NMC electrode to show a decreasing volume vs. Li extraction might be advantageous for the strain compensation created by C– $\text{Li}_x\text{C}_6$  volume difference (+10.6%) at least in part and, consequently, reduce the cyclic strain during the cell operation. The maximum in the *c/a* ratio (determined by selected material composition/adapted voltage window and being a favorable characteristic of selected cathode material from the safety point of view) for  $\text{Li}_x(\text{Ni}_{0.5}\text{Mn}_{0.3}\text{Co}_{0.2})\text{O}_2$  was found at ca. 90% SOC of the cell, which is quite close to the maximum of lattice parameter *c*.

In the discharged state of the cell the reversible cation mixing in form of  $((\text{Li}_{x-x'}\text{Ni}_{x'})_x(\text{Ni}_{0.5-x}\text{Li}_{x'}\text{Mn}_{0.3}\text{Co}_{0.2})\text{O}_2)$  was observed. The Li/Ni cation mixing ( $x' \sim 0.056(8)$  frac. un) has been found nearly capacity independent below 1600 mAh. Upon further charging (1800–2237 mAh) no cation mixing was observed leaving the  $\text{Li}_x(\text{Ni}_{0.5}\text{Mn}_{0.3}\text{Co}_{0.2})\text{O}_2$  structural formula for the cathode. In other words performed *in situ* NPD analysis revealed that Li loss from 3b layers occurs at moderate capacities resulting in no cation mixing in the cathode material at charges above 80% SOC.

Obtained results (in contrast to Refs. [44,45,48]) unambiguously showed the influence of cell charge on the cation mixing in nickel-rich NMC material and have been found in fair agreement to the observations from Refs. [46,47] stating that Li in  $\text{LiNi}_{0.5}\text{Mn}_{0.5}\text{O}_2$  is removed from transitional metal positions during charging. The observed independence of Ni/Li cation mixing magnitude within the range of its existence possibly enables its optimization (minimization) at the initial (lithium rich) state. However numerous degrees of freedom existing in NMC materials along with a not fully understood role of the cell formation call for more systematic studies of interactions in this system.

The critical lithium occupation  $x_{\text{Li}} \sim 0.4$  where lattice parameter *c* is maximal and cation mixing vanishes [35] can be associated with the superposition of structural contributions originating from changed oxidation states of transition metals, cation mixing and lithium concentration-driven changes in character of interatomic interactions, but its detailed origin can not be determined on the basis of the performed experiments with sufficient confidence and requires additional studies.

#### Acknowledgment

This work is financially supported by the Deutsche Forschungsgemeinschaft DFG as part of the Research Collaborative Centre 595 “Electrical fatigue in functional materials”. The authors thank to Andrea Voss (Institute for Complex Materials, IFW

Dresden) for the assistance with ICP-OES analysis of the electrode materials.

#### References

- [1] J.N. Reimers, J.R. Dahn, J. Electrochem. Soc. 139 (8) (1992) 2091–2096.
- [2] H. Abe, K. Zaghib, K. Tatsumi, S. Higuchi, J. Power Sources 54 (1995) 236–239.
- [3] G.G. Amatucci, J.M. Tarascon, L.C. Klein, J. Electrochem. Soc. 143 (3) (1996) 1114–1123.
- [4] M.A. Rodriguez, D. Ingersoll, D.H. Doughty, JCPDS Adv. X-ray Anal. 45 (2002) 182–187.
- [5] S. Laubach, S. Laubach, P.C. Schmidt, D. Ensling, S. Schmid, W. Jaegermann, A. Thissen, K. Nikolowski, H. Ehrenberg, Phys. Chem. Chem. Phys. 11 (2009) 3278–3289.
- [6] T. Ozuku, A. Ueda, M. Nagayama, Y. Iwakoshi, H. Komori, Electrochim. Acta 38 (1993) 1159–1167.
- [7] J. Barker, R. Koksang, M.Y. Saidi, Solid State Ionics 89 (1996) 25–35.
- [8] A. Rougier, P. Gravereau, C. Delmas, J. Electrochem. Soc. 143 (1996) 1168–1175.
- [9] C. Delmas, M. Menetrier, L. Croguennec, I. Saadoune, A. Rougiera, C. Pouillier, G. Prado, M. Gruene, L. Fournes, Electrochim. Acta 45 (1999) 243–253.
- [10] Y. Zhang, C.-Y. Wang, J. Electrochem. Soc. 156 (2009) A527–A535.
- [11] M.A. Rodriguez, M.H. Van Benthem, D. Ingersoll, S.C. Vogel, H.M. Reiche, Powder Diff. 25 (2) (2010) 143–148.
- [12] N. Sharma, V.K. Peterson, J. Solid State Electrochem. 16 (2012) 1849–1856.
- [13] N. Sharma, X. Guo, G. Du, Z. Guo, J. Wang, Z. Wang, V. Peterson, J. Am. Chem. Soc. 134 (2012) 7867–7873.
- [14] V.A. Godbole, M. Hess, C. Villevieille, H. Kaiser, J.-F. Colin, P. Novak, RSC Adv. 3 (2013) 757–763.
- [15] M. Roberts, J.J. Biendicho, S. Hull, P. Beran, T. Gustafsson, G. Svensson, K. Edström, J. Power Sources 226 (2013) 249–255.
- [16] S.-T. Myung, S. Komaba, N. Kumagai, Electrochim. Acta 47 (2002) 3287–3295.
- [17] L. Cai, K. An, Z. Feng, C. Liang, S.J. Harris, J. Power Sources 236 (2013) 163–168.
- [18] R.J. Gummov, A. de Kock, M.M. Thackeray, Solid State Ionics 69 (1994) 59–67.
- [19] H. Huang, P.G. Bruce, J. Power Sources 54 (1995) 52–57.
- [20] N. Yabuuchi, T. Ohzuku, J. Power Sources 119–121 (2003) 171–174.
- [21] H. Kobayashi, Y. Arachi, S. Emura, H. Kageyama, K. Tatsumi, T. Kamiyama, J. Power Sources 146 (2005) 640–644.
- [22] J. Choi, A. Manthiram, J. Electrochem. Soc. 152 (9) (2005) A1714–A1718.
- [23] S.-H. Park, H.-S. Shin, S.-T. Myung, C.S. Yoon, K. Amine, Y.-K. Sun, Chem. Mater. 17 (2005) 6–8.
- [24] N. Yabuuchi, Y. Koyama, N. Nakayama, T. Ohzuku, J. Electrochem. Soc. 152 (7) (2005) A1434–A1440.
- [25] X. Luo, X. Wang, L. Liao, S. Gamboa, P.J. Sebastian, J. Power Sources 158 (2006) 654–658.
- [26] Y. Idemoto, T. Matsui, Solid State Ionics 179 (2008) 625–635.
- [27] P. Samarasingha, D.-H. Tran-Nguyen, M. Behm, A. Wijayasinghe, Electrochim. Acta 53 (2008) 7995–8000.
- [28] N. Igawa, T. Taguchi, H. Fukazawa, H. Yamauchi, W. Utsumi, J. Am. Ceram. Soc. 93 (8) (2010) 2144–2146.
- [29] M. Ma, N.A. Chernova, B.H. Toby, P.Y. Zavalij, M.S. Whittingham, J. Power Sources 165 (2007) 517–534.
- [30] Y. Bentaleb, I. Saadoune, K. Maher, L. Saadi, K. Fujimoto, S. Ito, J. Power Sources 195 (2010) 1510–1515.
- [31] J.-M. Kim, H.-T. Chung, Electrochim. Acta 49 (2004) 937–944.
- [32] Y.-J. Gu, Y.-B. Chen, H.-Q. Liu, Y.-M. Wang, C.-L. Wang, H.-K. Wu, J. Alloys Compd. 509 (2011) 7915–7921.
- [33] E. Shinova, R. Stoyanova, E. Zhecheva, G.F. Ortiz, P. Lavela, J.L. Tirado, Solid State Ionics 179 (2008) 2198–2208.
- [34] J.-M. Kim, H.-T. Chung, Electrochim. Acta 49 (2004) 3573–3580.
- [35] Y.-S. Hong, Y.J. Park, K.S. Ryu, S.H. Chang, Y.-J. Shin, J. Power Sources 147 (2005) 214–219.
- [36] F. Weill, N. Tran, L. Croguennec, C. Delmas, J. Power Sources 172 (2007) 893–900.
- [37] X. Zhang, W.J. Jiang, A. Mauger, Qilu, F. Gendron, C.M. Julien, J. Power Sources 195 (2010) 1292–1301.
- [38] R. Santhanam, P. Jones, A. Sumana, B. Rambabu, J. Power Sources 195 (2010) 7391–7396.
- [39] D. Mohanty, S. Kalnaus, R.A. Meisner, K.J. Rhodes, J. Li, E.A. Payzant, D.L. Wood III, C. Daniel, J. Power Sources 229 (2013) 239–248.
- [40] Y. Wang, N. Sharma, D. Su, D. Bishop, H. Ahn, G. Wang, Solid State Ionics 233 (2013) 12–19.
- [41] J. Li, L. Wang, Q. Zhang, X. He, J. Power Sources 189 (2009) 28–33.
- [42] K. Shizuka, T. Kobayashi, K. Okahara, K. Okamoto, S. Kanzaki, R. Kanno, J. Power Sources 146 (2005) 589–593.
- [43] F. Wang, Y. Zhang, J. Zou, W. Liu, Y. Chen, J. Alloys Compd. 558 (2013) 172–178.
- [44] O. Sekizawa, T. Hasegawa, N. Kitamura, Y. Idemoto, J. Power Sources 196 (2011) 6651–6656.
- [45] Y. Arachi, H. Kobayashi, S. Emura, Y. Nakata, M. Tanaka, T. Asai, H. Sakaebe, K. Tatsumi, H. Kageyama, Solid State Ionics 176 (2005) 895–903.
- [46] W.-S. Yoon, Y. Paik, X.-Q. Yang, M. Balaasubramanian, J. McBreen, C.P. Grey, Electrochem. Solid-State Lett. 5 (11) (2002) A263–A266.

- [47] J. Breger, Y.S. Meng, Y. Hinuma, S. Kumar, K. Kang, Y. Shao-Horn, G. Ceder, C.P. Grey, *Chem. Mater.* 18 (2006) 4768–4781.
- [48] Y. Idemoto, Y. Takanashi, N. Kitamura, *J. Power Sources* 189 (2009) 269–278.
- [49] Z. Lu, J.R. Dahn, *J. Electrochem. Soc.* 149 (7) (2002) A815–A822.
- [50] P.-Y. Liao, J.-G. Duh, J.-F. Lee, H.-S. Sheu, *Electrochim. Acta* 53 (2007) 1850–1857.
- [51] K.-W. Nam, W.-S. Yoon, H. Shin, K.Y. Chung, S. Choi, X.-Q. Yang, *J. Power Sources* 192 (2009) 652–659.
- [52] T.E. Conry, A. Mehta, J. Cabana, M. Doeff, *Chem. Mater.* 24 (2012) 3307–3317.
- [53] W.K. Pang, N. Sharma, V.K. Peterson, J.-J. Shiu, S.-H. Wu, *J. Power Sources* 246 (2014) 464–472.
- [54] H. Liu, C.R. Fell, K. An, L. Cai, Y.S. Meng, *J. Power Sources* 240 (2013) 772–778.
- [55] H. Berg, J.O. Thomas, *Solid State Ionics* 126 (1999) 227–234.
- [56] H. Berg, H. Rundlöv, J.O. Thomas, *Solid State Ionics* 144 (2001) 65–69.
- [57] N. Sharma, G. Du, A.J. Studer, Z. Guo, V.K. Peterson, *Solid State Ionics* 199–200 (2011) 37–43.
- [58] A. Senyshyn, M.J. Mühlbauer, K. Nikolowski, T. Pirling, H. Ehrenberg, *J. Power Sources* 203 (2012) 126–129.
- [59] M.A. Rodriguez, D. Ingersoll, S.C. Vogel, D.J. Williams, *Electrochem. Solid-State Lett.* 7 (1) (2004) A8–A10.
- [60] N. Sharma, V.K. Peterson, M.M. Elcombe, M. Avdeev, A.J. Studer, N. Blagojevic, R. Yusoff, N. Kamarulzaman, *J. Power Sources* 195 (2010) 8258–8266.
- [61] O. Dolotko, A. Senyshyn, M.J. Mühlbauer, K. Nikolowski, F. Scheiba, H. Ehrenberg, *J. Electrochem. Soc.* 159 (12) (2012) A2082–A2088.
- [62] Senyshyn, O. Dolotko, M.J. Mühlbauer, K. Nikolowski, H. Fuess, H. Ehrenberg, *J. Electrochem. Soc.* 160 (5) (2013) A3198–A3205.
- [63] N. Sharma, V.K. Peterson, *Electrochim. Acta* 101 (2013) 79–85.
- [64] C.-W. Hu, N. Sharma, C.-Y. Chiang, H.-C. Su, V.K. Peterson, H.-W. Hsieh, Y.-F. Lin, W.-C. Chou, B.-Y. Shew, *J. Power Sources* 244 (2013) 158–163.
- [65] L. Liang, S.H. Lee, H.S. Choi, B.S. Seong, C.W. Yi, K. Kim, in: 216-th Meeting of Electrochemical Society, 4–9 October 2009, Vienna, Austria, Conference Abstract, vol. 902(8), 2009, p. 549.
- [66] N. Sharma, V.K. Peterson, *J. Power Sources* 244 (2013) 695–701.
- [67] X.-L. Wang, K. An, L. Cai, Z. Feng, S.E. Nagler, C. Daniel, K.J. Rhodes, A.D. Stoica, H.D. Skorpenske, C. Liang, W. Zhang, J. Kim, Y. Qi, S.J. Harris, *Sci. Rep.* 2 (2012) 747, 1–7.
- [68] M. Hoelzel, A. Senyshyn, N. Juenke, H. Boysen, W. Schmahl, H. Fuess, *Nucl. Instrum. Methods A* 667 (2012) 32–37.
- [69] T. Roisnel, J. Rodriguez-Carvajal, *Mater. Sci. Forum* 378–381 (2001) 118–123.
- [70] M. Winter, J.O. Besenhard, M.E. Spahr, P. Novak, *Adv. Mater.* 10 (10) (1998) 725–763.
- [71] J.O. Besenhard, H.P. Fritz, *Angew. Chem. Int. Ed. Engl.* 22 (1983) 950–975.
- [72] T. Ohzuku, Y. Iwakoshi, K. Sawai, *J. Electrochem. Soc.* 140 (9) (1993) 2490–2498.
- [73] J.R. Dahn, *Phys. Rev. B* 44 (1991) 9170–9177.
- [74] T.A. Hewston, B.L. Chamberland, *J. Phys. Chem. Solids* 48 (2) (1987) 97–108.
- [75] A. Van der Ven, M.K. Aydinol, G. Ceder, G. Kresse, J. Hafner, *Phys. Rev. B* 58 (6) (1998) 2975–2987.